NASA Technical Memorandum 87579

Semiempirical Method for Predicting Vortex-Induced Rolling Moments

Dennis O. Allison and Percy J. Bobbitt

NOVEMBER 1985

NASA

NASA Technical Memorandum 87579

Semiempirical Method for Predicting Vortex-Induced Rolling Moments

Dennis O. Allison and Percy J. Bobbitt
Langley Research Center
Hampton, Virginia

National Aeronautics
and Space Administration

**Scientific and Technical
Information Branch**

1985

SUMMARY

A method is described herein for the prediction of rolling moments on a wing penetrating a vortex velocity field generated by a large aircraft. Rolling moments are determined from lifting pressure coefficients computed with an inviscid-flow linear panel method. Two empirical corrections are included to account for the lifting efficiency of an airfoil section and the local stall on the wing. Predicted rolling moments are compared with those from two wind-tunnel experiments. Results indicate that experimental rolling moments, for which the Reynolds number of the following wing is low, should be interpreted with caution.

INTRODUCTION

One of the greatest hazards to a small aircraft in an airport environment is a strong rolling moment induced by an axial penetration of a wake vortex produced by a large aircraft. Determination of the induced rolling moment is, therefore, a vital part of the study of the wake vortex hazard. The effectiveness of a given vortex attenuator can be studied by measuring the vortex velocity distributions in the wake of an aircraft with and without the attenuator and calculating the relative rolling moments produced on a following aircraft.

The validation of a predictive method requires measured wake velocity distributions as well as induced rolling moments on a wing in the same wake. However, only a limited amount of data is available which includes both measurements. References 1 to 3 present this type of data as well as some comparisons with applicable theories. Predicted rolling-moment results from two-dimensional strip theory, strip theory with an empirical lift-curve slope correction, and vortex-lattice theory are presented in reference 1. In reference 2 rolling moments are predicted with simple strip theory in which the local lift-curve slope is assumed to be the same as the overall measured lift-curve slope and the lift is limited to a maximum value. Inviscid-flow rolling-moment results from lifting-line theory are presented in reference 3. The present approach (with a linear panel method) involves corrections based on measured airfoil data for both local lift-curve slope and local stall (maximum lift).

The purpose of this paper is to present a method for computing the rolling moment for an axial penetration of a wing into a vortex whose velocity distribution is known. Since the method accounts for variations with Reynolds number, it can be useful in the interpretation of wind-tunnel data. Development of the method was stimulated by work in the Langley Vortex Research Facility (refs. 4 and 5) and by the introduction of the laser-velocimeter technique (ref. 6) for measurement of velocity distributions. Results in the present paper are compared with experimental data from references 2 and 3.

SYMBOLS

a	area of finite-element panel, in^2
B	span of vortex-generating wing, in.
b	span of following wing, in.
C_l	rolling-moment coefficient (eq. (1))
C_L	lift coefficient of vortex-generating wing
c	chord of following wing, in.
c_l	section lift coefficient
c_{l_α}	section lift-curve slope, per deg
F	section lift factor (eq. (7))
R_c	Reynolds number based on chord of following wing
S	following-wing planform area, in^2
V/U_∞	ratio of vortex velocity to free-stream velocity
x	rectangular coordinate in streamwise direction, in.
y	rectangular coordinate in spanwise direction, in.
α	angle of attack, deg
α_{es}	effective stall angle (eq. (8)), deg
ΔC_p	lifting pressure coefficient on a finite-element panel

Subscripts:

exp	experimental
i	summation index on wing panels
L	left group of finite-element panels
max	maximum
o	centerline of following wing
R	right group of finite-element panels

A prime on a symbol indicates the value is calculated from inviscid-flow linear theory for a flat-plate wing; a bar over a symbol indicates a coordinate at the centroid of area of the finite-element panel.

METHOD

A vortex velocity field imposes a torque which causes an aircraft encountering the vortex to roll. For an axial penetration, the initial rolling moment is the maximum value. Throughout the present paper, the term "rolling moment" means "initial rolling moment."

The rolling moment on a wing in an axial encounter with a wake vortex can be approximated fairly well by inviscid-flow steady-state theory (ref. 7), but only for very large Reynolds numbers. Inviscid-flow calculations are not sufficient for predicting the rolling moment in a wind tunnel where the Reynolds number of the following wing is very low. The steady-state method described herein includes empirical corrections to account for the effects of Reynolds number and of airfoil camber and thickness on the lift an airfoil section can attain. A computer program by Carmichael et al. (ref. 8) for inviscid linear-theory flow over wing-body combinations is used to calculate the pressure distribution on a flat-plate wing which is modeled by a number of finite-element panels. An input modification allows for the nonuniformity (vortex velocity distribution) in the incoming airstream and for local stall ($c_{l,max}$) on the wing. A section lift factor is used to account for the experimental lifting efficiency (c_{l_α}) of the airfoil. The resulting wing pressure distribution is used in the computation of the rolling-moment coefficient.

The effect of the following wing on the vortex velocity distribution is not considered in the present work. The fuselage is not modeled and Mach number effects are not taken into account. Also, post-stall lift loss is not considered in the local stall correction.

Wake Vortex Simulation

The effect of a nonsymmetrical vortex velocity distribution (e.g., fig. 1) on a following wing is accounted for by imposing an artificial twist distribution on the wing. The local wing incidence is the sum of the angle of attack α, the geometric twist angle, and the artificial twist angle (arctan (V/U_∞)). To account for stall, the local wing incidence is limited by the angle corresponding to $c_{l,max}$ for the test Reynolds number based on the following-wing chord.

The linear-theory aerodynamics program (ref. 8) models a wing with a number of constant-pressure panels. It requires the geometry of a semispan wing as input and automatically reflects across a plane of symmetry to account for the other half of the wing. (See example in fig. 2(a).) Therefore, any twist distribution specified by program inputs appears symmetrically in the reflected geometry. The appropriate nonsymmetrical twist distribution cannot be imposed on the wing in the usual way. Therefore, the input wing is taken as the entire wing so that a nonsymmetrical twist distribution can be applied as needed. The aerodynamic interference from the reflected wing must be reduced by moving the input wing away from the program symmetry plane (fig. 2(b)). At a separation distance of 10 wing spans (fig. 2(c)) the interference between the input and reflected wings results in less than 0.1 percent error in the lifting pressure coefficients. A separation distance of 10 or more wing spans is used in practice to ensure negligible interference between the wing of interest and its reflected image. A large spearation distance is achieved by simply adjusting inputs to the program.

Rolling-Moment Coefficient

The rolling-moment coefficient is computed from the lifting pressure coefficient ΔC_p and the spanwise rectangular coordinate of the centroid of area $\bar{y}$ for each of the 100 finite-element panels that make up the input wing. Five panels are used in the chordwise direction and numbered as shown in figure 3(a). Since the input wing is taken as the entire wing, the panels are renumbered into a left group and a right group, as shown in figure 3(b). Thus,

$$C_l = C_{l,L} + C_{l,R} \tag{1}$$

The contribution from the left group is

$$C_{l,L} = \frac{-1}{Sb} \sum_{i=1}^{50} (\Delta C_p)_{L,i} a_{L,i} (\bar{y}_{L,i} - y_o) \tag{2}$$

Similarly,

$$C_{l,R} = \frac{-1}{Sb} \sum_{i=1}^{50} (\Delta C_p)_{R,i} a_{R,i} (\bar{y}_{R,i} - y_o) \tag{3}$$

The lifting pressure coefficients are determined from the section lift factor F (which is explained in the next section) and lifting pressure coefficients calculated from inviscid-flow linear theory on a flat-plate wing:

$$(\Delta C_p)_{L,i} = F(\Delta C_p')_{L,i} \tag{4}$$

and

$$(\Delta C_p)_{R,i} = F(\Delta C_p')_{R,i} \tag{5}$$

Since the constant F is a factor in all terms of equation (1),

$$C_l = FC_l' \tag{6}$$

Empirical Corrections

Two empirical corrections are included in the rolling-moment coefficient; one corrects the airfoil section lift-curve slope and the other allows for local stall on the wing. The two corresponding parameters are the section lift factor F and the effective stall angle α_{es}. These parameters can be determined from curves for airfoil experimental c_l as a function of α from sources such as references 9 to 11.

Section lift factor.- The section lift factor F is the ratio of $(c_{l_\alpha})_{exp}$ to c'_{l_α}, where $c'_{l_\alpha} = 0.094$ is calculated at the center of a rectangular wing of aspect ratio 1000 with no twist. Therefore,

$$F = (c_{l_\alpha})_{exp}/0.094 \tag{7}$$

and accounts for viscosity and for airfoil camber and thickness. Consider an NACA 0012 airfoil at a low Reynolds number. The plot of experimental c_l as a function of α is shown in figure 4 for this airfoil at the lowest test Reynolds number (R_c = 170 000) for which NACA 0012 data are given in reference 9. Note that the curve is linear with $(c_{l_\alpha})_{exp} = 0.100$ below $\alpha = 5^o$. Therefore, $F = 0.100/0.094 = 1.06$ in this example. This factor corrects the calculated c_l so that it agrees with experiment at low angles of attack and follows the line of long dashes in figure 4.

Effective stall angle.- The effective stall angle is

$$\alpha_{es} = (c_{l,max})_{exp}/(c_{l_\alpha})_{exp} \tag{8}$$

For the rolling-moment calculation, α_{es} is used to limit the calculated c_l to the experimental maximum. For the curve in figure 4, $(c_{l,max})_{exp} = 0.83$ as shown by the line of short dashes. Thus, from equation (8), $\alpha_{es} = 0.83/0.100 = 8.3^o$. (See intersection of dashed lines.) Since the airfoil is symmetric, $\alpha_{es} = -8.3^o$ for negative angles of attack. For a cambered airfoil, a different α_{es} would have to be determined for negative angles of attack. To account for stall on the wing penetrating the vortex, the local wing incidence (geometric plus vortex-induced incidence) is limited to the effective stall angle. Consider a penetrating (following) wing with no geometric incidence ($\alpha = 0$ and no twist), so that the local wing incidence is simply arctan (V/U_∞). For the vortex velocity distribution from figure 1 and a symmetric airfoil with $\alpha_{es} = 10^o$, figure 5 shows how the tangent of α_{es} limits the vortex velocity distribution.

RESULTS AND DISCUSSION

Two cases are treated based on availability of relevant experimental data. Both are for a central penetration of a vortex by a wing with $\alpha = 0$, no geometric twist, and a symmetric airfoil section. In each case, two Reynolds numbers are considered; one is higher than the experimental value and the other is near the experimental value. The effects of F and α_{es} are studied by computing rolling-moment coefficients with and without these empirical corrections. Predicted results are presented with no corrections, with one correction, and with both corrections, and results are compared with experimental data. As noted earlier, verification of the present method requires experimental data for which rolling-moment coefficients and corresponding vortex velocity distributions are known. The effect of the following wing on the vortex velocity distribution is not considered. Airfoil-section data of the following wing must also be known or calculable. Results are computed for one case from reference 2 and for one case from reference 3.

Case A

Measured velocity distributions are given in reference 2 for trailing vortices at $x/B = 2.5$ and $x/B = 5.0$ behind a 35^o sweptback wing with $B = 42.00$ in. for lift coefficients of $C_L = 0.36$ and $C_L = 0.74$. The distribution with the highest maximum velocity, namely, that for $x/B = 2.5$ and $C_L = 0.74$, is used for case A.

(See fig. 1.) The rectangular following wing with an aspect ratio of 7.5 has an NACA 64_2-015 airfoil section with roughness to fix transition, $b = 10.00$ in., $c = 1.33$ in., and $R_c \approx 110\ 000$ in the experiment.

For $R_c = 6\ 000\ 000$ and the NACA 64_2-015 airfoil, $(c_{l_\alpha})_{exp} = 0.110$ and $(c_{l,max})_{exp} = 1.10$ from the standard-roughness lift curve in reference 10. From equations (7) and (8), $F = 0.110/0.094 = 1.17$ and $\alpha_{es} = 1.10/0.110 = 10^o$. ($\alpha_{es} = -10^o$ for negative α.) As shown in figure 6, F increases the uncorrected rolling-moment coefficient from 0.070 to 0.082 and α_{es} decreases it from 0.082 to 0.080 for $R_c = 6\ 000\ 000$. (Compare figs. 1 and 5 to see the cause for this small decrease.)

Since no experimental lift curve is known to be available for the NACA 64_2-015 airfoil with roughness for a Reynolds number near $R_c = 110\ 000$, corresponding estimates of $(c_{l_\alpha})_{exp}$ and $(c_{l,max})_{exp}$ are now made. The ratio of the maximum lift coefficients at two Reynolds numbers is assumed to be the same for rough or smooth symmetric airfoils with the same thickness-to-chord ratio. Lift curves are available in reference 10 for the NACA 64_2-015 airfoil with and without roughness for $R_c = 6\ 000\ 000$ and without roughness for $R_c = 3\ 000\ 000$. As shown in this reference, $(c_{l,max})_{exp} = 1.33$ for $R_c = 3\ 000\ 000$ and $(c_{l,max})_{exp} = 1.45$ for $R_c = 6\ 000\ 000$ without roughness. Therefore, $(c_{l,max})_{exp} \approx 1.10(1.33/1.45) = 1.01$ for a rough NACA 64_2-015 airfoil at $R_c = 3\ 000\ 000$. For another smooth 15-percent-thick symmetric airfoil, namely, an NACA 0015 (ref. 9), $(c_{l,max})_{exp} = 0.83$ for $R_c = 84\ 000$ and $(c_{l,max})_{exp} = 1.55$ for $R_c = 3\ 260\ 000$. Linear interpolations between these values give $(c_{l,max})_{exp} = 0.84$ for $R_c = 110\ 000$ and $(c_{l,max})_{exp} = 1.49$ for $R_c = 3\ 000\ 000$. Therefore, $(c_{l,max})_{exp} \approx 1.01(0.84/1.49) = 0.57$ for NACA 64_2-015 with roughness for $R_c = 110\ 000$. Since the lift-curve slope is not sensitive to Reynolds number, it is estimated to be $(c_{l_\alpha})_{exp} \approx 0.110$ (same as for the higher Reynolds number). Therefore, $F \approx 1.17$ and $\alpha_{es} \approx 0.57/0.110 = 5^o$. The rolling-moment coefficient for this combination of parameters is below that for the higher Reynolds number and is more in line with the experimental result of reference 2 (fig. 6).

Case B

Velocity distributions of single and interacting trailing vortices and rolling moments on a following model measured in a wind tunnel are reported in reference 3. A measured velocity distribution for a merged vortex formed from two corotating equal-strength vortices (fig. 7) is used for case B since a corresponding measured C_l is given more accurately than others in reference 3. The velocity distribution is measured at $x/B = 8.49$ downstream of two semispan wings with $B = 28.50$ in. The rectangular following-wing model with an aspect ratio of 5.2 has an NACA 0012 airfoil section, $b = 4.56$ in., $c = 0.87$ in., and $R_c \approx 50\ 000$ in the experiment.

For the NACA 0012 airfoil at the highest test Reynolds number ($R_c = 3\ 180\ 000$) in reference 9, $(c_{l_\alpha})_{exp} = 0.103$ and $(c_{l,max})_{exp} = 1.56$. Therefore, $F = 0.103/0.094 = 1.10$ and $\alpha_{es} = 1.56/0.103 = 15^o$ ($\alpha_{es} = -15^o$ for negative α). As shown

in figure 8, F increases C_l from 0.130 to 0.143, but stall has no effect since the local incidence (arctan (V/U_∞)) does not exceed α_{es}. (See fig. 7.)

For $R_c = 43\ 000$ (the lowest test Reynolds number in reference 9 for the NACA 0009 and NACA 0015 airfoils), $(c_{l_\alpha})_{exp} = 0.100$ and $(c_{l,max})_{exp} = 0.80$ are average values from NACA 0009 and NACA 0015 data. Therefore, $F = 0.100/0.094 = 1.06$ and $\alpha_{es} = 0.80/0.100 = 8^o$. As shown in figure 8, F increases C_l from 0.130 to 0.138, whereas $\alpha_{es} = 8^o$ significantly decreases it from 0.138 to 0.100, as might be expected from figure 7.

Case B can be used to point out a potential problem with the interpretation of wind-tunnel results for low Reynolds numbers. The predicted $C_l = 0.143$ for $R_c = 3\ 180\ 000$ (fig. 8) is much higher than the experimental result. On the other hand, the predicted C_l of 0.100 for $R_c = 43\ 000$ (which is near the experimental $R_c = 50\ 000$) is below the experimental result. These results indicate the rolling-moment coefficient for $R_c = 3\ 180\ 000$ is about 40 percent higher than that for $R_c = 43\ 000$. In other words, the rolling moment in flight may be much higher than that measured at a low Reynolds number in a wind tunnel.

CONCLUDING REMARKS

A method of computing rolling-moment coefficients for axial penetrations into a wake vortex is described in terms of simple modifications to a computer program which calculates wing-body aerodynamics. Wing twist is used to make allowances for the nonuniformity of the incoming airstream without considering the effects of the following wing on the vortex velocity distribution. Any computer program for subsonic wing aerodynamics for uniform free-stream flow can be modified in a similar way, provided that it has the capability of treating an arbitrary twist distribution across the full span of the wing. A program which treats arbitrary twist on an input semispan wing and reflects it across a plane of symmetry can also be used, provided that the input wing geometry can be separated arbitrarily far away from any reflected geometry. A section lift factor and an effective stall angle are used to make corrections for viscosity as well as for airfoil camber and thickness.

The results of this method can be useful in studying the relative hazards of wakes from various vortex-generating aircraft configurations and in assessing and understanding the effect of stall on wind-tunnel results. Measurements of rolling moment for low Reynolds numbers can be misleading if stall occurs on the following wing. Flight data for higher Reynolds numbers will be less influenced by flow separation and may result in higher rolling moments.

NASA Langley Research Center
Hampton, VA 23665-5225
August 1, 1985

REFERENCES

1. Rossow, Vernon J.; Corsiglia, Victor R.; Schwind, Richard G.; Frick, Jaunita K. D.; and Lemmer, Opal J.: Velocity and Rolling-Moment Measurements in the Wake of a Swept-Wing Model in the 40- by 8-Foot Wind Tunnel. NASA TM X-62414, 1975.

2. El-Ramly, Z.; Rainbird, W. J.; and Earl, D. G.: Some Wind Tunnel Measurements of the Trailing Vortex Development Behind a Sweptback Wing: Induced Rolling Moments on Intercepting Wings. AIAA Paper No. 75-884, June 1975.

3. Iversen, J. D.; Corsiglia, V. R.; Park, S.; Backhus, D. R.; and Brickman, R. A.: Hot-Wire, Laser Anemometer and Force Balance Measurements of Cross-Sectional Planes of Single and Interacting Trailing Vortices. AIAA Paper 78-1194, July 1978.

4. Patterson, James C., Jr.; and Jordan, Frank L., Jr.: An Investigation of the Increase in Vortex Induced Rolling Moment Associated With Landing Gear Wake. NASA TM X-72786, 1975.

5. Patterson, James C., Jr.; and Jordan, Frank L., Jr.: Thrust-Augmented Vortex Attenuation. Wake Vortex Minimization, NASA SP-409, 1977, pp. 251-270.

6. Gartrell, Luther R.; and Rhodes, David B.: A Scanning Laser-Velocimeter Technique for Measuring Two-Dimensional Wake-Vortex Velocity Distributions. NASA TP-1661, 1980.

7. Rossow, Vernon J.: Inviscid Modeling of Aircraft Trailing Vortices. Wake Vortex Minimization, NASA SP-409, 1977, pp. 9-59.

8. Carmichael, Ralph L.; Castellano, Charles R.; and Chen, Chuan F.: The Use of Finite Element Methods for Predicting the Aerodynamics of Wing-Body Combinations. Analytic Methods in Aircraft Aerodynamics, NASA SP-228, 1970, pp. 37-51.

9. Jacobs, Eastman N.; and Sherman, Albert (appendix by Ira H. Abbott): Airfoil Section Characteristics as Affected by Variations of the Reynolds Number. NACA Rep. 586, 1937.

10. Abbott, Ira H.; Von Doenhoff, Albert E.; and Stivers, Louis S., Jr.: Summary of Airfoil Data. NACA Rep. 824, 1945. (Supersedes NACA WR L-560.)

11. Miley, S. J.: A Catalog of Low Reynolds Number Airfoil Data for Wind Turbine Applications. RFP-3387 (Subcontract No. PFY12781-W, Contract No. DE-AC04-76DP03533), Dep. Aerospace Eng., Texas A&M Univ., Feb. 1982.

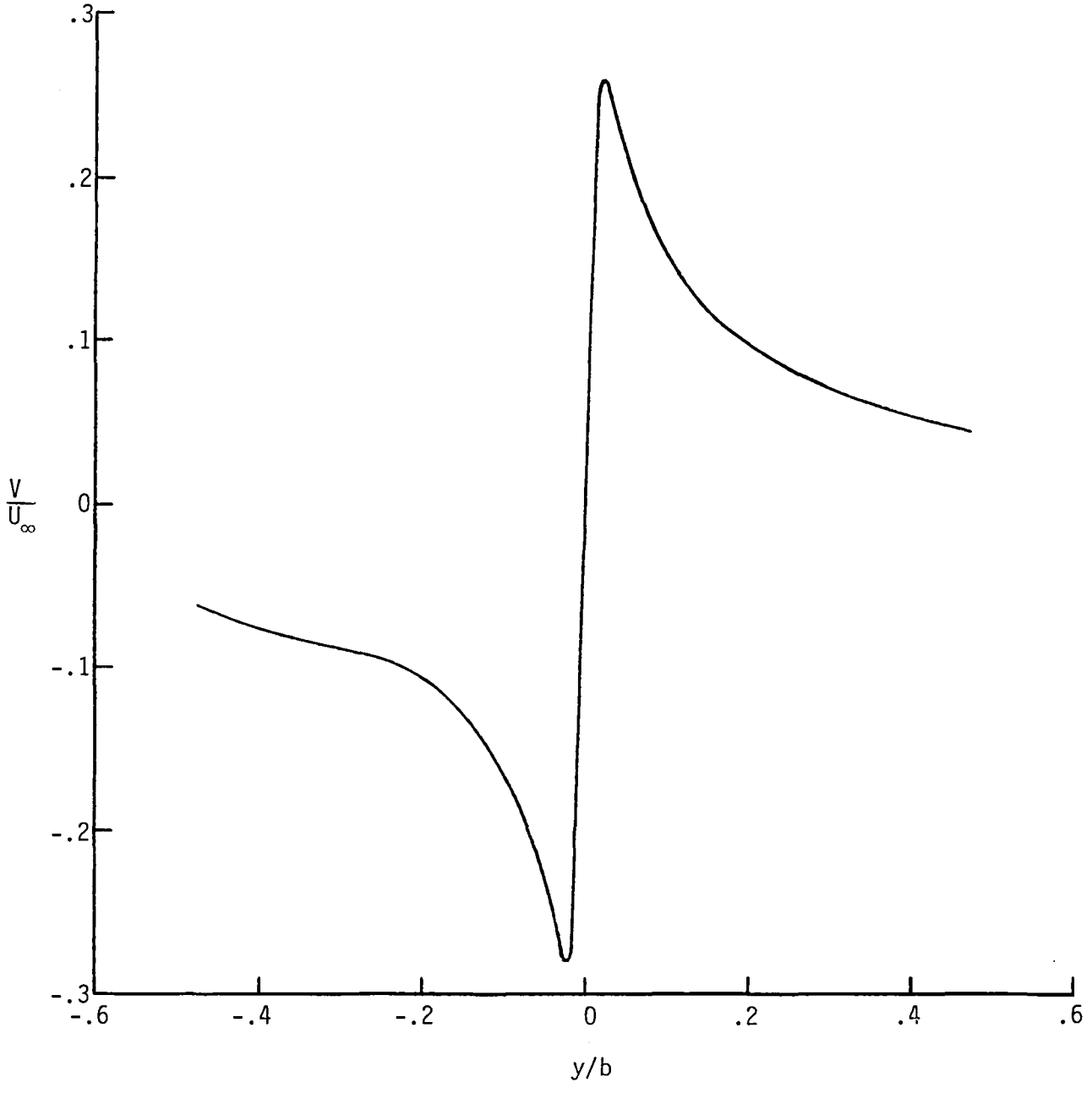

Figure 1.- Vortex velocity distribution measured in wind tunnel at x/B = 2.5 behind 35° sweptback wing with C_L = 0.74 (ref. 2).

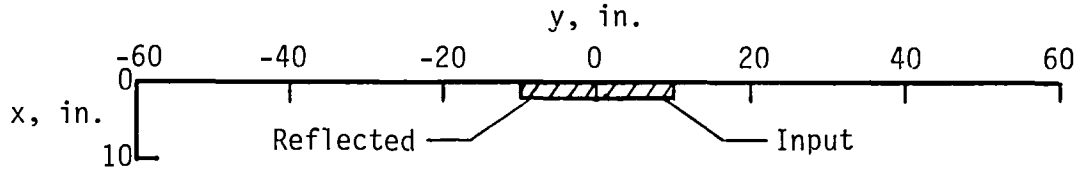

(a) Strong aerodynamic interference with no separation.

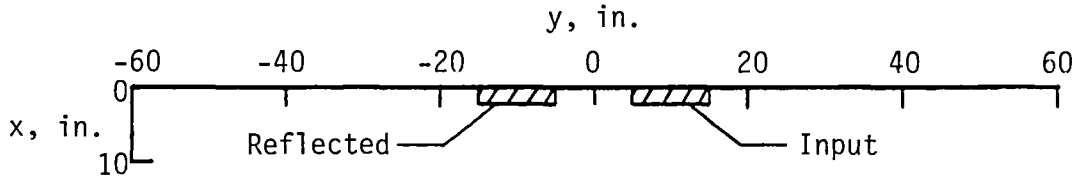

(b) Weak aerodynamic interference with separation of 1 span.

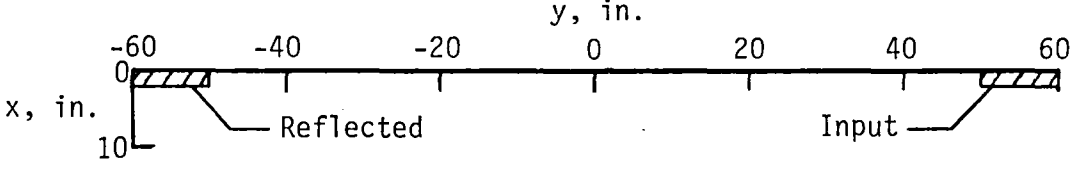

(c) Negligible aerodynamic interference with separation of 10 spans.

Figure 2.- Effect of separation distance on interference between input and reflected wings (top view).

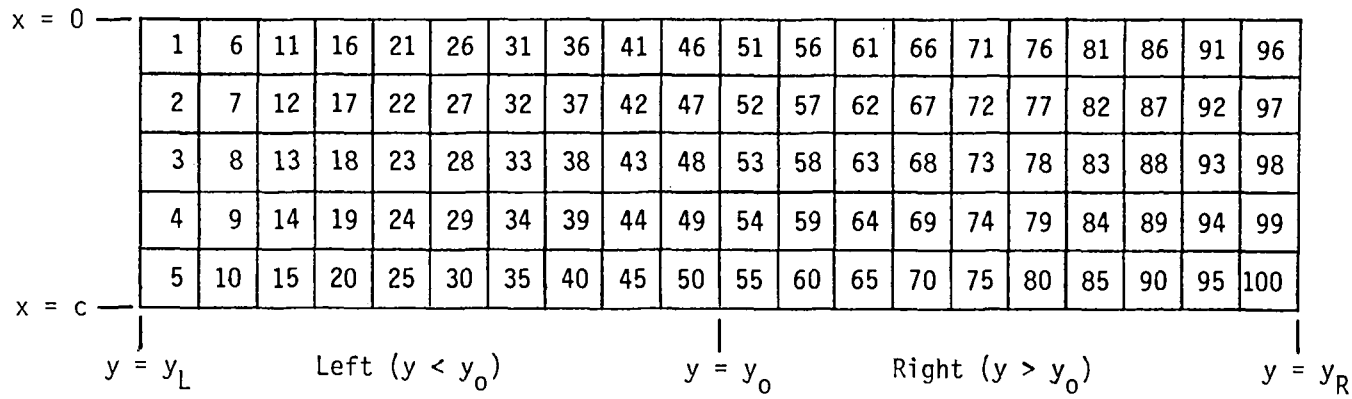

1	6	11	16	21	26	31	36	41	46	51	56	61	66	71	76	81	86	91	96
2	7	12	17	22	27	32	37	42	47	52	57	62	67	72	77	82	87	92	97
3	8	13	18	23	28	33	38	43	48	53	58	63	68	73	78	83	88	93	98
4	9	14	19	24	29	34	39	44	49	54	59	64	69	74	79	84	89	94	99
5	10	15	20	25	30	35	40	45	50	55	60	65	70	75	80	85	90	95	100

(a) Original numbering system for wing panels.

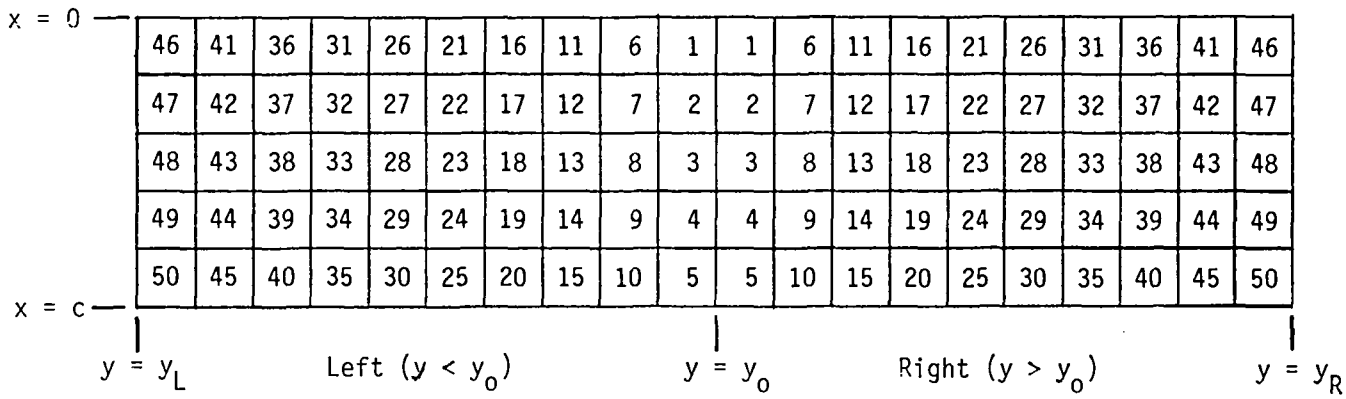

46	41	36	31	26	21	16	11	6	1	1	6	11	16	21	26	31	36	41	46
47	42	37	32	27	22	17	12	7	2	2	7	12	17	22	27	32	37	42	47
48	43	38	33	28	23	18	13	8	3	3	8	13	18	23	28	33	38	43	48
49	44	39	34	29	24	19	14	9	4	4	9	14	19	24	29	34	39	44	49
50	45	40	35	30	25	20	15	10	5	5	10	15	20	25	30	35	40	45	50

(b) Panels renumbered into left and right groups.

Figure 3.- Numbering system of panels on input wing.

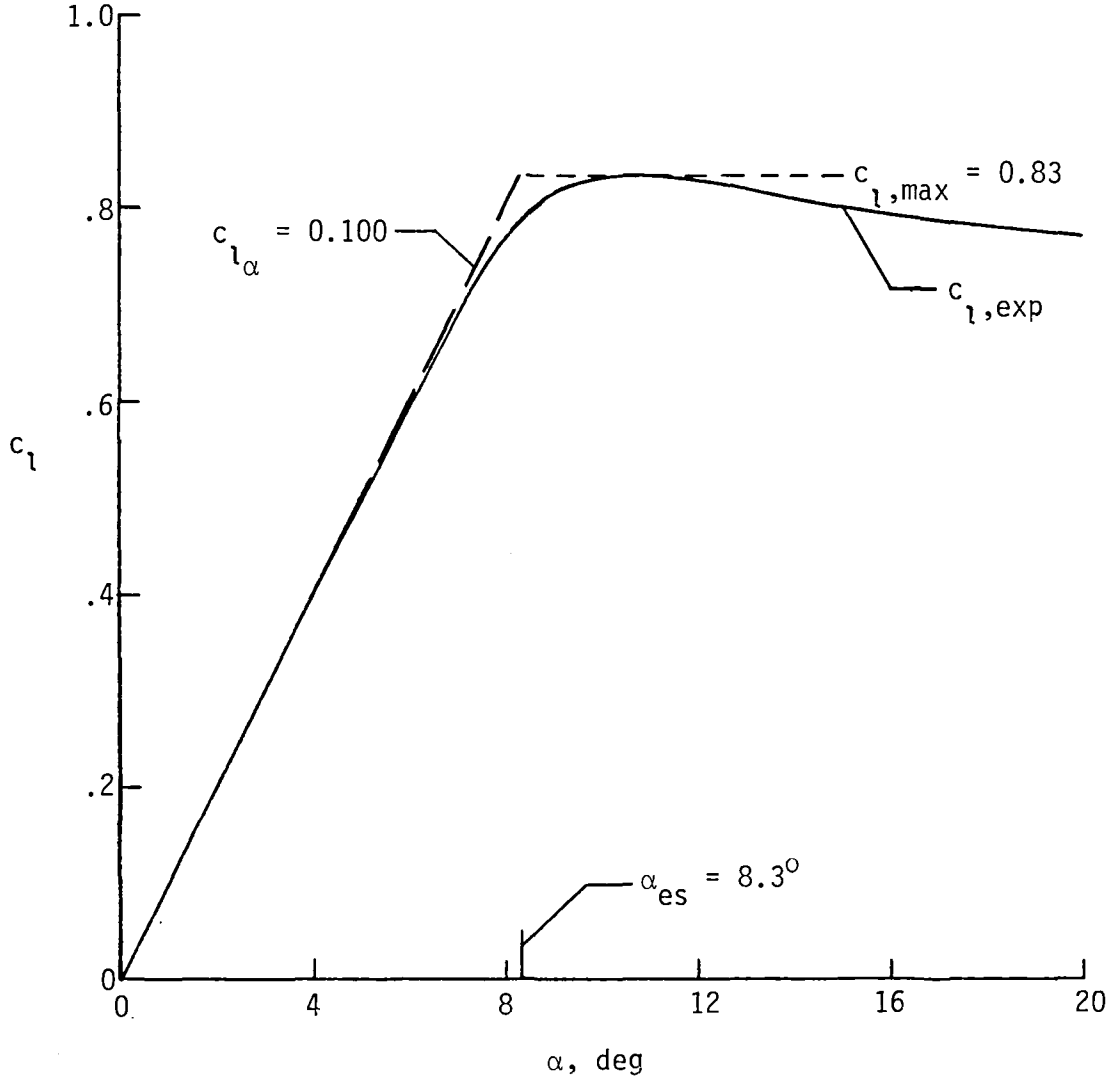

Figure 4.- Section lift curve measured in wind tunnel for NACA 0012 airfoil at R_c = 170 000 (ref. 9).

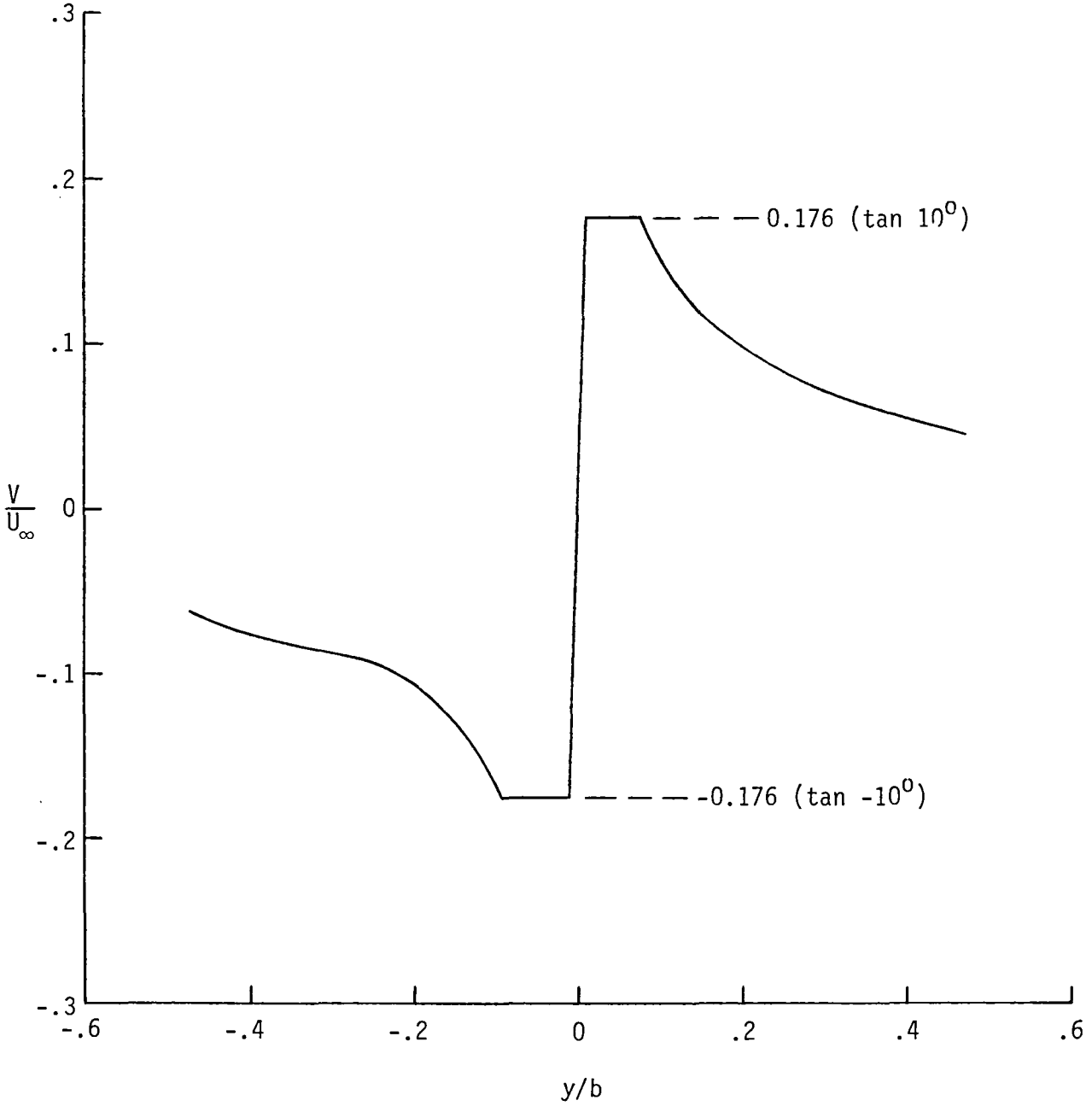

Figure 5.- Vortex velocity distribution in figure 1 adjusted for an effective stall angle of 10°.

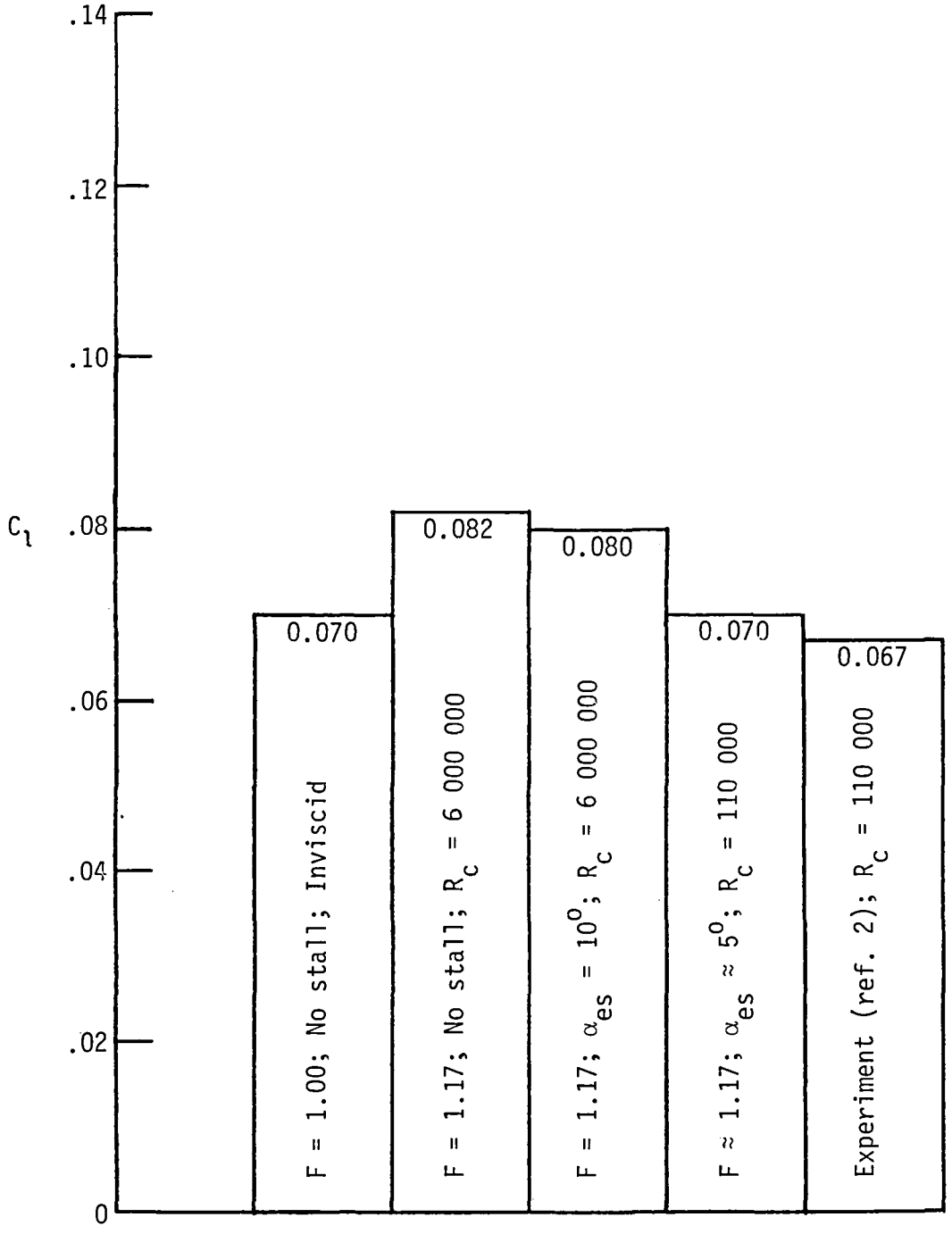

Figure 6.- Effect of corrections on rolling-moment coefficient for following-wing model with aspect ratio of 7.5 for vortex velocity distribution in figure 1 (case A).

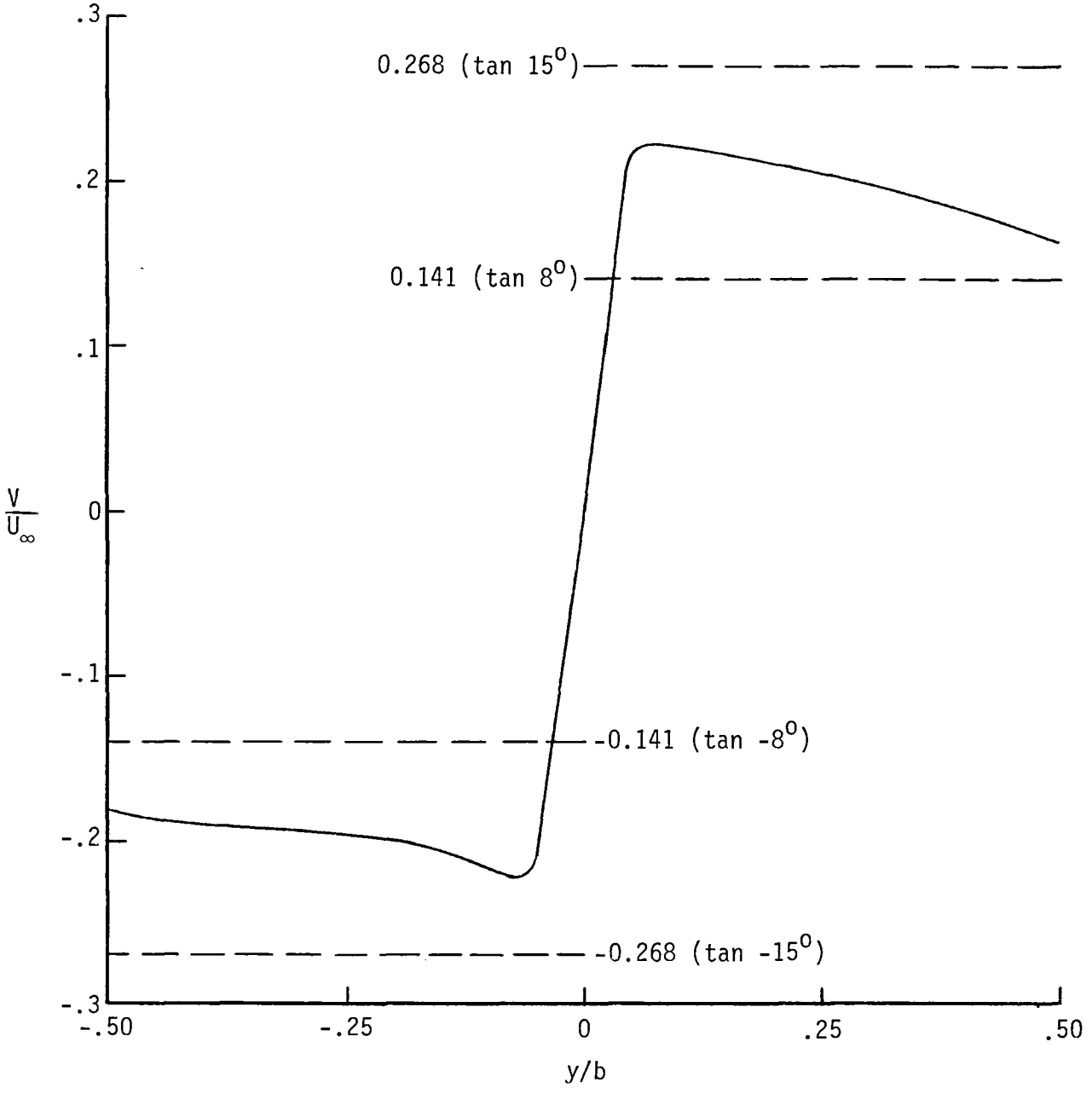

Figure 7.- Velocity distribution of merged vortex measured in wind tunnel at x/B = 8.49 downstream of two semispan wings (ref. 3).

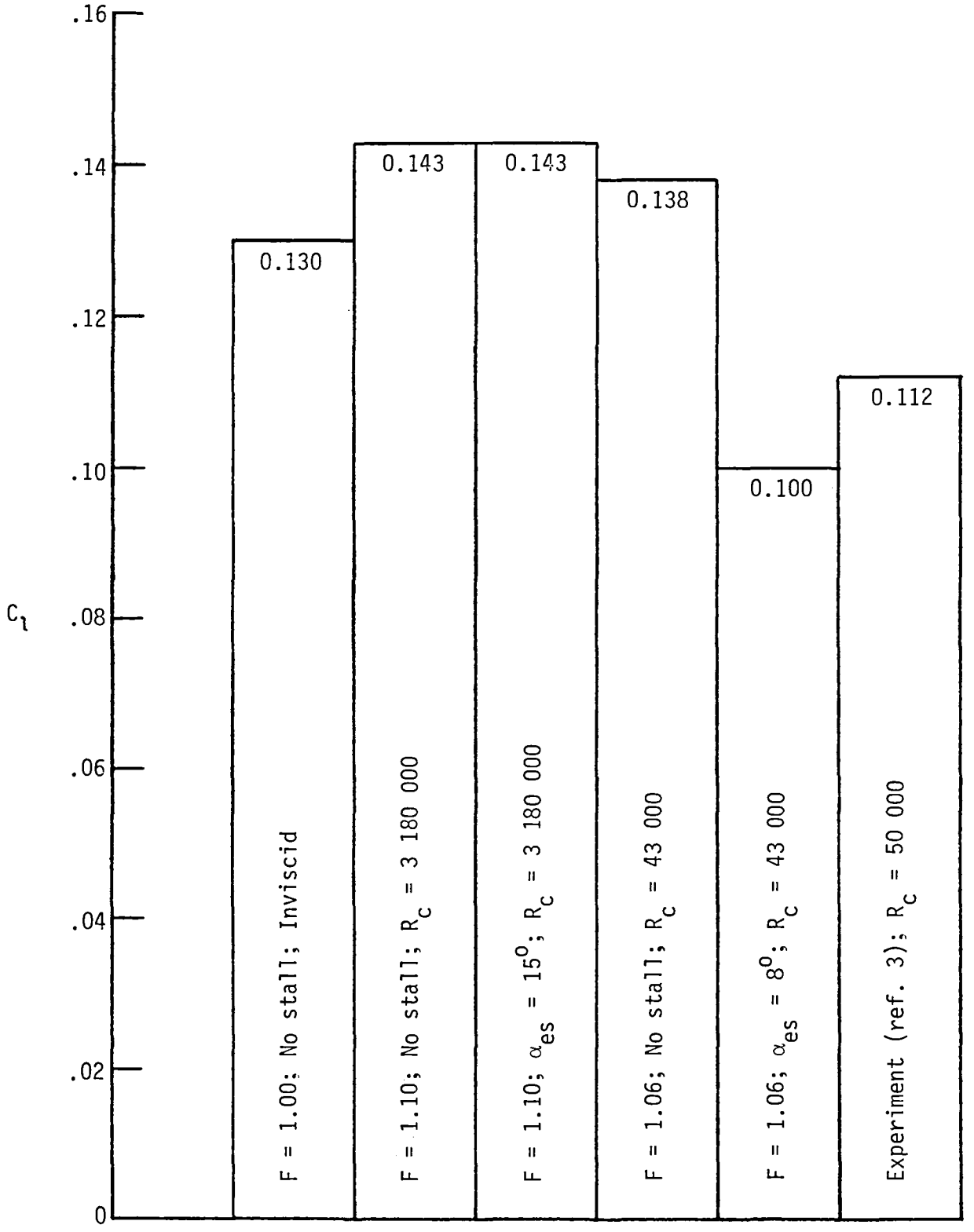

Figure 8.- Effect of corrections on rolling-moment coefficient for following-wing model with aspect ratio of 5.2 for vortex velocity distribution in figure 7 (case B).

1. Report No.	2. Government Accession No.	3. Recipient's Catalog No.
NASA TM-87579		

4. Title and Subtitle	5. Report Date
Semiempirical Method for Predicting Vortex-Induced Rolling Moments	November 1985
	6. Performing Organization Code: 505-43-90-04
7. Author(s)	8. Performing Organization Report No.
Dennis O. Allison and Percy J. Bobbitt	L-15986
9. Performing Organization Name and Address	10. Work Unit No.
NASA Langley Research Center Hampton, VA 23665-5225	11. Contract or Grant No.
12. Sponsoring Agency Name and Address	13. Type of Report and Period Covered
National Aeronautics and Space Administration Washington, DC 20546-0001	Technical Memorandum
	14. Sponsoring Agency Code

15. Supplementary Notes

16. Abstract

A method is described for the prediction of rolling moments on a wing penetrating a vortex velocity field generated by a large aircraft. Rolling moments are determined from lifting pressure coefficients computed with an inviscid-flow linear panel method. Two empirical corrections are included to account for the lifting efficiency of an airfoil section and the local stall on the wing. Predicted rolling moments are compared with those from two wind-tunnel experiments. Results indicate that experimental rolling moments, for which the Reynolds number of the following wing is low, should be interpreted with caution.

17. Key Words (Suggested by Authors(s))	18. Distribution Statement
Rolling moment Semiempirical method Wake vortex Vortex velocity distribution Effective stall angle	Unclassified - Unlimited Subject Category 02

19. Security Classif.(of this report)	20. Security Classif.(of this page)	21. No. of Pages	22. Price
Unclassified	Unclassified	17	A02

For sale by the National Technical Information Service, Springfield, Virginia 22161

NASA-Langley, 1985

National Aeronautics and
Space Administration
Code NIT-4

Washington, D.C.
20546-0001